Boundary-Layer Meteorol (2018) 166:51–68
https://doi.org/10.1007/s10546-017-0296-4

RESEARCH ARTICLE

Observations of Wind-Direction Variability in the Nocturnal Boundary Layer

Francisco Lang[1] · **Danijel Belušić**[2] · **Steven Siems**[3]

Received: 11 January 2017 / Accepted: 14 August 2017 / Published online: 7 September 2017

Abstract Large sudden wind-direction shifts and submeso variability under nocturnal conditions are examined using a micrometeorological network of stations in north-western Victoria, Australia. The network was located in an area with mostly homogeneous and flat terrain. We have investigated the main characteristics of the horizontal propagation of events causing the wind-direction shift and not addressed in previous studies. The submeso motions at the study site exhibit behaviour typical of flat terrain, such as the lower relative mesovelocity scale and smaller cross-wind variances than that for complex terrain. The distribution of wind-direction shifts shows that there is a small but persistent preference for counter-clockwise rotation, occurring for 55% of the time. Large wind-direction shifts tend to be associated with a sharp decrease in air temperature (74% of the time), which is associated with rising motion of cold air, followed by an increase in turbulent mixing. The horizontal propagation of events was analyzed using the cross-correlation function method. There is no preferred mean wind direction associated with the events nor is there any relationship between the mean wind and propagation directions. The latter indicates that the events are most likely not local flow perturbations advected by the mean flow but are rather features of generally unknown origin. This needs to be taken into account when developing parametrizations of the stable boundary layer in numerical models.

Keywords Microfronts · Propagation of structures · Stable boundary layer · Submeso motions · Wind-direction shifts

✉ Francisco Lang
francisco.lang@monash.edu

[1] School of Earth, Atmosphere and Environment, Monash University, Clayton, VIC, Australia

[2] Rossby Centre, Swedish Meteorological and Hydrological Institute, Nörrkoping, Sweden

[3] School of Earth, Atmosphere and Environment, Monash University and Australian Research Council Centre of Excellence for Climate System Science, Clayton, VIC, Australia

1 Introduction

Over land under nocturnal conditions and relatively clear skies, the net radiative cooling of the ground induces a positive vertical temperature gradient, which generates a stable atmospheric boundary layer (ABL) (Mahrt 2014). Even with the prevalence of the stable ABL, and the existence of many studies that have examined its behaviour, the knowledge of fundamental features remains incomplete (Sun et al. 2015b). The behaviour of turbulent and non-turbulent motions in the stable ABL is not well described by the classical theories of the ABL, and this lack of understanding increases with stability (Grachev et al. 2005; Acevedo et al. 2014; Mahrt 2014; Kang et al. 2015; Vercauteren and Klein 2015).

The very stable ABL does not categorically satisfy traditional definitions of turbulence (Mahrt 2014). Under very stable conditions, the turbulence is highly intermittent and is associated with non-stationary processes (Sun et al. 2015b), and small-scale non-turbulent motions govern the environment (Vickers et al. 2008). In this regard, the turbulence time and length scales may be restricted to very small values; in very stable conditions, the turbulent processes may have an upper time scale limit of between 5 and 10 s (Acevedo et al. 2014). Such small time scales relate to a spectrum of generally unknown motions, which separate turbulence scales from the mesoscale (Belušić and Mahrt 2012; Vercauteren et al. 2016). Motions in this range have been termed submesoscale (or submeso) and are loosely defined as non-turbulent atmospheric motions on scales larger than seconds, but smaller than those traditionally classified as mesoscale (Belušić and Mahrt 2008; Acevedo et al. 2014; Sun et al. 2015b). Such a loose definition could be given in terms of space scales, although there is a general understanding that submeso motions do not follow the Taylor hypothesis, and knowledge of them derives from point measurements. Submeso motions exist under all atmospheric conditions, but are very important when the mean flow is weak (Vickers et al. 2008; Cava et al. 2016; Mortarini et al. 2016). With low wind speeds they become the dominant motion pattern, produce sudden and large wind-direction shifts, and influence mixing and fluxes of scalars and momentum. The above definition is broad and considers processes with different physical origins that may coexist in the nocturnal ABL (Acevedo et al. 2014). The high variability of submeso processes seems to be influenced in a complex way by local surface features, such as terrain and vegetation (Monti et al. 2002; Vickers and Mahrt 2007).

Only a few studies have analyzed abrupt and large wind-direction shifts under stable conditions. Mahrt (2007, 2008) analyzed wind-direction variability from different field experiments and found that changes in wind direction at low wind speeds are more often abrupt shifts rather than gradual meandering of the wind vector. These studies conclude that abrupt changes in wind direction are associated with a wide variety of phenomena and are not systematically related to changes in turbulence intensity or changes of other variables, except for a slight tendency for the development of larger wind-direction shifts with the passage of cold microfronts.

Since sudden wind-direction shifts occur predominantly at low wind speeds and are prone to high concentrations of atmospheric pollutants due to low mixing and ventilation (Vickers et al. 2008), they may have a considerable impact on air quality. However, sudden submeso wind-direction shifts are currently not reproduced or parametrized in numerical models (Belušić and Güttler 2010; Güttler and Belušić 2012; Suarez et al. 2015), and an understanding of their generation remains incomplete (Mahrt 2008). Some of the ubiquitous problems related to modelling the stable ABL in numerical weather prediction and climate models (e.g., Sandu et al. 2013) may be related to the absence of a treatment of submeso processes.

Mahrt (2014) specifically identified the parametrization of the change in wind direction as a challenge in the simulation of horizontal dispersion.

The main goal of our study is to examine submeso variability and large sudden wind-direction shifts under nocturnal conditions using a micrometeorological network of stations. The network allows us to characterize the horizontal propagation of events causing the wind-direction shifts, which has not been addressed previously. We attempt to answer the following questions:

- Can we confirm that the submeso wind-direction variability is related to local terrain characteristics?
- Are submeso motions advected by, or at least related to, the local mean flow?
- Can we gain any insight into their spatial scales from point observations?
- Hence, could submeso motions be parametrized locally?

The paper is structured as follows: the dataset, study area and methods are described in Sect. 2, and the general statistics of submeso motions are presented and compared with other field experiments in Sect. 3. Section 4 analyzes the characteristics and effects of large sudden wind-direction shifts, and in Sect. 5 the horizontal propagation of events causing wind-direction shifts is estimated and compared to the mean flow. Section 6 provides conclusions.

2 Data and Methods

2.1 Data

The field experiment was designed to characterize the submeso motions that are not generated by terrain or surface heterogeneity, to the maximally achievable extent considering the ubiquitous heterogeneity of the land surface. The wind and temperature data were collected from a micrometeorological network composed of four towers that form an equilateral Y-shaped horizontal array with a radius of 580 m (Fig. 1), positioned within a large area with predominantly homogeneous and flat terrain in north-western Victoria, Australia. The terrain has a small slope towards the south (less than 0.05% within 10 km around the network). In addition, there is a 20-m high hill approximately 15 km north-east of the network, and a 30-m high hill about 30 km to the south-west. The horizontal network of high-resolution measurements was designed to cover the typical range of horizontal scales of submeso structures in the ABL. The main tower was located at the centre of the network (main station; 35°52′5.89″S, 143°20′35.96″W). It was instrumented with a three-dimensional Campbell Scientific CSAT3 sonic anemometer at 3 m above the ground sampling at 10 Hz, and slow response wind and temperature sensors at 6 m above the ground sampling with a 1-min interval. The three satellite towers were instrumented with two-dimensional Gill WindSonic sonic anemometers at 3 m above the ground sampling at 4 Hz. The three-dimensional sonic data were tilt-corrected using the planar fit method (Wilczak et al. 2001).

The experiment was conducted from 23 March 2013 to 25 January 2015; however, the main station only operated from 23 March 2013 to 19 June 2013 due to technical problems. Since only the main station was equipped with a three-dimensional anemometer, we focus the analysis on the latter shorter period, except when specifically noted otherwise. Following similar analysis in Mahrt (2008), the data between 2000 LST and 0800 LST the next day were used for the analysis in order to remove daytime conditions.

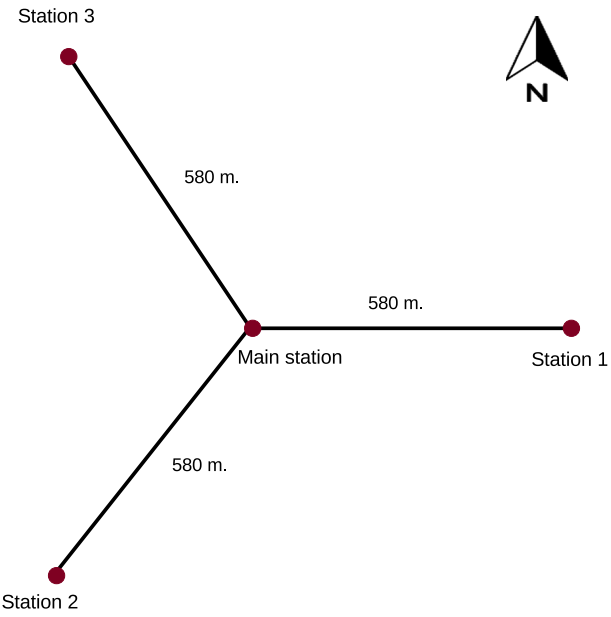

Fig. 1 The schematic of the micrometeorological network in north-western Victoria, Australia

2.2 Methods

We use three different methodologies for investigating the submeso motions and wind-direction variability: a bulk approach analyzing the statistics of the entire dataset, an approach based on extracting all individual structures that cause large and sudden wind-direction shifts, and finally an analysis of the propagation of these structures.

2.2.1 Submeso Motions

Two measures of submeso motions are used here to compare our field experiment with previous studies, corresponding to the cross-wind velocity variance and the mesovelocity scale.

The contribution to the cross-wind velocity variance from submeso motions is a typical measure of the plume spread, and we use the method of Vickers and Mahrt (2007) to calculate the cross-wind velocity variance. They defined this as the difference between the total variance at averaging time scale τ and the variance due to turbulent motions alone. For the purpose of comparison with Vickers and Mahrt (2007), the coordinate system was rotated such that the 4-h average v-component was zero, in order to obtain the cross-wind component. With the same purpose, the contribution of turbulent motions was fixed to the scale of 5 min, and different time scales τ used to calculate the velocity variance are shown in Table 1. As discussed in Vickers and Mahrt (2007) and Mahrt (2008), the final statistics depend strongly on the choice of averaging time, which is why we closely repeated their procedure.

A measure of the strength of the submeso flow, called the mesovelocity scale, is defined by Mahrt (2007) as

$$V_{meso} \equiv \left[\left(\tilde{v}^2 + \tilde{u}^2\right)^{1/2}\right], \tag{1}$$

Table 1 Mean (standard deviation in parenthesis) of the log base 10 of the submeso cross-wind velocity variance ($m^2\ s^{-2}$) for averaging times τ of 15, 60 and 240 min

Site	Class	15	60	240
Victoria	Weakly stable	−1.43 (0.34)	−0.85 (0.39)	−0.44 (0.46)
	More stable	−1.52 (0.31)	−0.98 (0.34)	−0.67 (0.38)
FLOSSII	Weakly stable	−0.76 (0.41)	−0.21 (0.45)	0.17 (0.48)
	More stable	−0.85 (0.34)	−0.34 (0.33)	−0.04 (0.36)
CASES-99	Weakly stable	−1.46 (0.46)	−0.99 (0.40)	−0.59 (0.47)
	More stable	−1.71(0.38)	−1.13 (0.42)	−0.71 (0.44)

The values from Vickers and Mahrt (2007) for FLOSSII and CASES-99 are included for comparison

where the tilde indicates the deviations of 1-min averages from the 1-h record average and the brackets refer to averaging over the 1-h record (Mahrt 2008). The choice of 1 min as the time scale is thoroughly discussed in Mahrt (2007). Note that although this measure is originally termed the mesovelocity scale, it may refer to submeso scales given the loose definition of submeso used above. In addition, the relative strength of the submeso flow is defined as

$$RV_{meso} = \frac{V_{meso}}{V}, \tag{2}$$

where V is the 1-h average wind speed. According to Mahrt (2007), wind-direction statistics can be related to RV_{meso}, and it was shown for the Fluxes Over Snow Surfaces II (FLOSSII) experiment that maximum wind-direction shifts increase with increasing RV_{meso} (Mahrt 2008). Values of $RV_{meso} > 1$ indicate a significant influence of submeso motions on the total velocity vector, yet $RV_{meso} < 1$ might still indicate important contributions from submeso motions.

2.2.2 Wind-Direction Shifts

Wind-direction variability is analyzed through sudden changes of wind direction, changes that are very common under low wind speeds in the stable ABL (Mahrt 2010). Wind-direction shifts are defined as the difference between the subsequent 1-min wind direction and the previous 1-min wind direction, implying that the differences are centred across 2-min intervals

$$\Delta WD_i = WD_{i+1} - WD_{i-1}, \tag{3}$$

where $\Delta WD_i \in [-180, 180]$. Mahrt (2008) notes that the variability of the wind direction decreases as the averaging length increases and the smallest submeso motions are eliminated. In order to detect large sudden shifts from the time series, we define "events" at the main station as $\Delta WD > 60°$. To analyze how these events are related to other variables before and after the wind-direction shift, we define time windows or sampling windows centred around the events. Different lengths of sampling windows were tested, and the length of 20 min (10 min before and after the events) was chosen as best suited for our goals. This sampling length also provides a sufficient number of points to study the propagation of structures (see the following sub-section). Sampling windows are extracted from the time series through an iterative process, and the first extracted sample is centred around the largest ΔWD within the entire dataset. Wind-direction shifts within this sampling window are then removed from further iteration. The next sample is centred around the largest ΔWD in the remaining dataset,

and so on. Since a sampling window can contain more than one event, the number of sampling windows is smaller than the number of events.

2.2.3 Propagation of Structures

We use the 20-min sampling windows surrounding wind-shift events to study the propagation of structures. The method for propagation is based on the cross-correlation function method (Rees and Mobbs 1988), which calculates the speed and direction of propagation between any three meteorological stations in a triangle. Given the stations 1, 2 and 3 with coordinates (x_1, y_1), (x_2, y_2) and (x_3, y_3), and time lags τ_{12}, τ_{13} and τ_{23}, respectively, assuming a disturbance with inverse period f passing through the three stations, the following relationships for the inverse horizontal wavelengths (k, ℓ) hold (Rees and Mobbs 1988):

$$kx_1 + \ell y_1 = kx_2 + \ell y_2 - f\tau_{12}, \tag{4}$$

$$kx_1 + \ell y_1 = kx_3 + \ell y_3 - f\tau_{13}. \tag{5}$$

Equations 4 and 5 can be solved for k and ℓ, hence the speed v_p and direction α of propagation can be determined (Monserrat and Thorpe 1992). Therefore,

$$k = \frac{f\{\tau_{12}(y_1 - y_3) - \tau_{13}(y_1 - y_2)\}}{(x_1 - x_3)(y_1 - y_2) - (x_1 - x_2)(y_1 - y_3)}, \tag{6}$$

$$\ell = \frac{f\{\tau_{13}(x_1 - x_2) - \tau_{12}(x_1 - x_3)\}}{(x_1 - x_3)(y_1 - y_2) - (x_1 - x_2)(y_1 - y_3)}, \tag{7}$$

$$v_p = \frac{f}{\sqrt{k^2 + \ell^2}}, \tag{8}$$

$$\alpha = 180^\circ + \tan^{-1}|k/\ell| \quad \text{if } k > 0,\ \ell > 0, \tag{9}$$

$$\alpha = 180^\circ - \tan^{-1}|k/\ell| \quad \text{if } k < 0,\ \ell > 0, \tag{10}$$

$$\alpha = 0^\circ + \tan^{-1}|k/\ell| \quad \text{if } k < 0,\ \ell < 0, \tag{11}$$

$$\alpha = 360^\circ - \tan^{-1}|k/\ell| \quad \text{if } k > 0,\ \ell < 0. \tag{12}$$

Note that since k and ℓ are linear functions of f (Eqs. 6, 7), then Eqs. 8–12 show that v_p and α are not functions of f. The angle α is defined as if measured from the north toward the direction of propagation. In order to have a consistent definition with the wind direction, α is later rotated to the standard meteorological convention.

Sampling windows are extracted from the three satellite stations over the same time periods as for the main station. An arbitrary example of a sampling window is shown in Fig. 2, illustrating a central event at the main station and its development through the network. To calculate the time lags between stations, the wind components were averaged to 10 s. A number of different averages were tried, and the 10-s average was found to perform best at removing small-scale variability while maintaining the main features of wind-direction shifts. The time lags between the stations of the network are determined using the maximum cross-correlation. In order to improve accuracy of the time-lag estimates, we use both horizontal wind components and the mean wind speed in calculations of the cross-correlation. From the four stations, six pairs of maximum cross-correlation coefficients and the corresponding time lags are obtained for each variable. The value of 0.7 is defined as the lower limit for the maximum cross-correlation coefficient using trial and error. Cases with two or more maximum cross-correlation coefficients from the six pairs that are above this limit are considered for propagation estimation. To choose among the available variables the one that

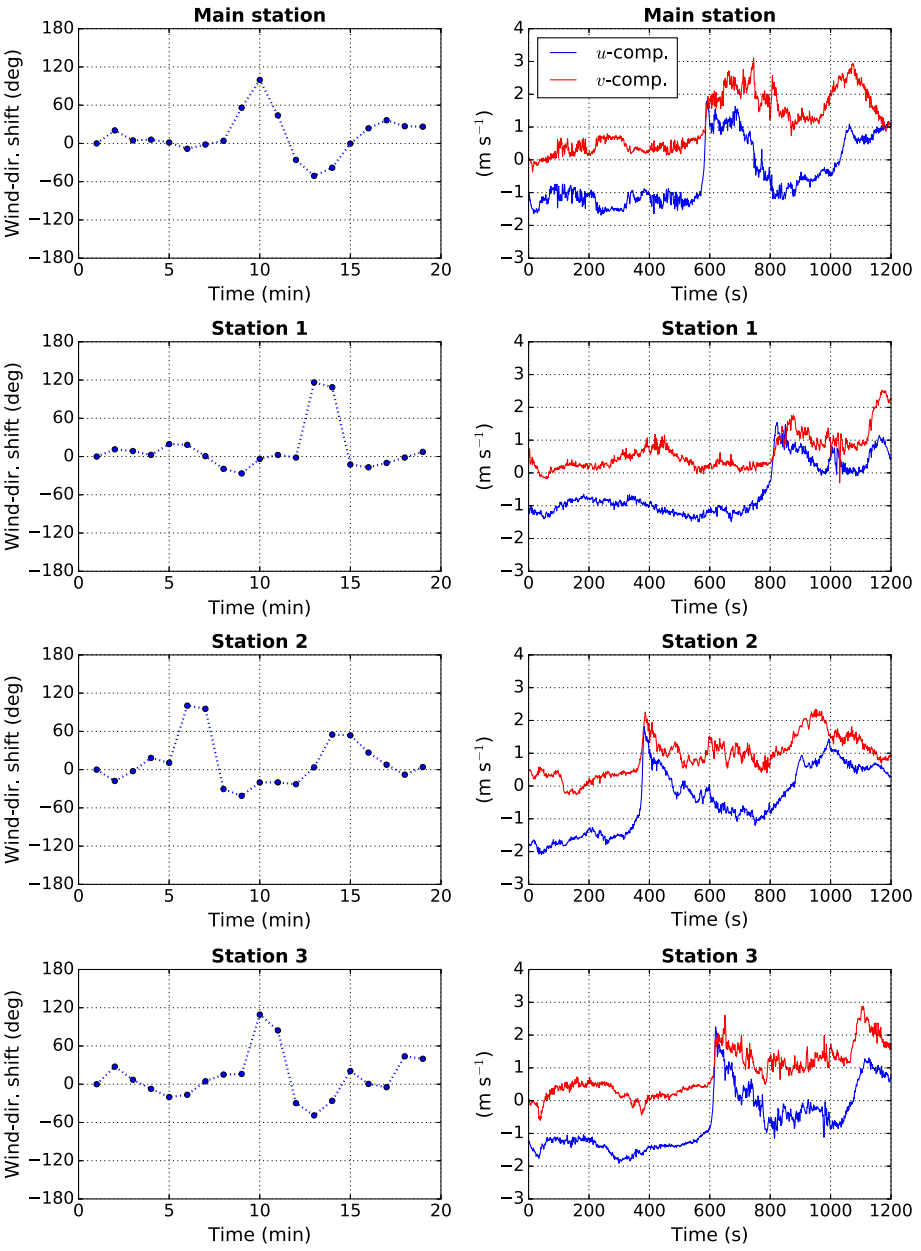

Fig. 2 An example of a sampling window for all the stations of the network: the wind-direction shifts (*left panels*) and 1-s averages (for display purposes) of the horizontal velocity components (*right panels*)

will be used to estimate the speed and direction of propagation for a particular case, the variable with the greatest maximum cross-correlation coefficient averaged over the six pairs of stations is chosen.

Table 2 Site name of field experiments, surface conditions, height of the sensor above the ground in metres, percentage of records with $RV_{meso} > 1$, and percentage of records with a wind-direction shift of 90° or larger

Site	sfc.	h	$RV_{meso} > 1$	Shift > 90°
Victoria	Grass/crops	3	3	14
FLOSSII	Grass/snow	2	14	23
CASES-99	Grass	5	2	16

3 Submeso Statistics

Here we calculate different measures of submeso variability and compare them with other field experiments and previous publications.

3.1 Cross-Wind Velocity Variance

While hereafter we use the entire nocturnal period, the stable conditions are quantified using the dimensionless stability parameter z/L, where z is the measurement height and L is the Obukhov length. For determining L, the turbulent fluctuations are calculated as deviations from the 5-min mean and the averaging time for fluxes is 4 h, which is consistent with the definition of the cross-wind velocity variance. This is done for the purpose of consistent comparison with the results of Vickers and Mahrt (2007). Following Vickers and Mahrt (2007), two classes of stable conditions are defined: the first with $0 < z/L < 0.1$ for weakly stable conditions, and the second with $0.1 < z/L < 2$. The mean and standard deviation of the cross-wind variance for different averaging lengths and two stability classes are shown in Table 1.

Vickers and Mahrt (2007) analyzed the cross-wind velocity variance for nine datasets in the USA and found that the variance was larger in complex terrain compared to flatter terrain and near homogeneous sites. Table 1 shows the cross-wind velocity variance for two of these datasets: FLOSSII, which lies in a complex terrain setting, and the Cooperative Atmosphere-Surface Exchange Study (CASES-99) (Poulos et al. 2002), which is over a relatively flat and homogeneous grass-covered terrain. Our homogeneous site has variances similar to CASES-99 and other such sites from Vickers and Mahrt (2007), which agrees with the hypothesis that the terrain complexity influences the submeso motions.

3.2 Mesovelocity Scale

The two additional datasets are used here as well to compare the overall statistics of RV_{meso} for stable conditions between different sites (Table 2). In the FLOSSII experiment, $RV_{meso} > 1$ occurs 14% of the time. On the other hand, for a flatter-terrain site, such as in CASES-99, this reduces to 2% of the time. Although the variability even between similar sites is generally large, $RV_{meso} > 1$ occurs 3% of the time for our site, which is comparable to a flatter site such as that at CASES-99.

4 Wind-Direction Shifts

4.1 Frequency Distribution of Wind-Direction Shifts

A total of 381 events were detected at the main station over the 89 nights, leading to 130 samples using the 20-min sampling window. There are usually two or more events in each

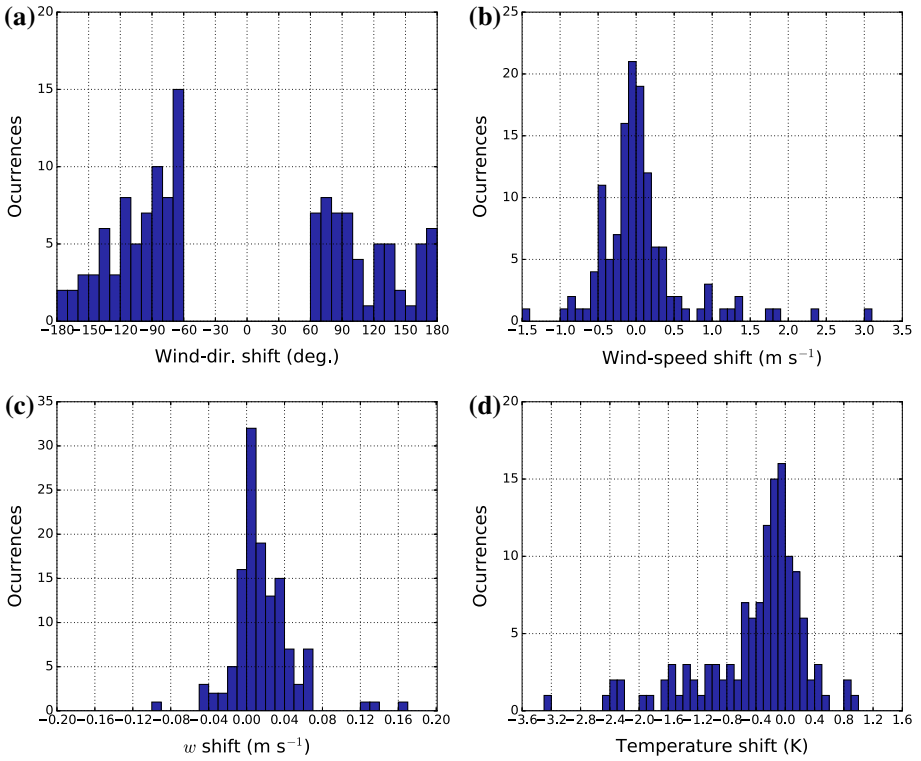

Fig. 3 Distribution of changes of the **a** wind direction, **b** wind speed, **c** vertical velocity component (w), and **d** temperature for the central events detected at the main station

sample, suggesting that isolated events are not common. We use only the central values of wind-direction-shifts within a sample, together with other available variables, to investigate the characteristics of 130 wind-direction-shift events.

The distribution of wind-direction shifts in Fig. 3a shows that there are 72 negative shifts (counter-clockwise rotation) and 58 positive shifts (clockwise rotation). The preference for counter-clockwise rotation is robust to the changes of the period of analysis, so there are more negative shifts during the longer 22-month period too, with the ratio of negative to positive shifts increasing with ΔWD. It could be hypothesized that the events resulting from downward mixing would have a tendency for counter-clockwise rotation in the Southern Hemisphere due to the possible Ekman turning in the ABL or due to the local acceleration resulting from vertical convergence of the momentum flux (Hande et al. 2012; Sun et al. 2013), while other mechanisms would not show such a preference. The samples were first separated according to the direction of rotation and analyzed separately. However, no significant structural difference between clockwise and counter-clockwise wind-direction shifts was detected, so we continue the analysis on all the samples together and return to the question of direction of rotation later. The central events are characterized by wind speeds below $1.5\,\mathrm{m\,s^{-1}}$ in 95% of the cases. This is in agreement with Anfossi et al. (2005), who defined wind speeds $<1.5\,\mathrm{m\,s^{-1}}$ as weak flow, with significant mesoscale variability of the wind direction occurring when the large-scale flow was weak.

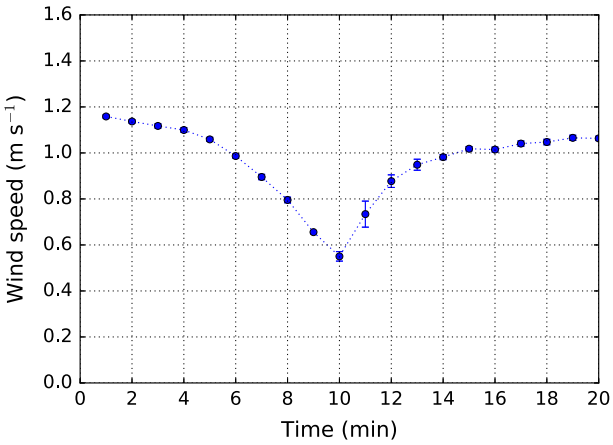

Fig. 4 Composite structure of mean wind speed for the central events detected at the main station. Error bars show ± one standard error

Changes in the wind speed during a central event are shown in Fig. 3b. Slightly more events (53%) are characterized with an increase of wind speed, and most of the changes are small, with values below 0.5 m s^{-1}. These changes, however, are defined by a centred difference over each 2-min interval. As such, they do not capture any transient fluctuations within this 2-min window including at the exact time of the event. To illustrate this, Fig. 4 shows the composite mean wind speed over all samples, indicating a considerable decrease of mean wind speed during a wind-direction shift. This decrease is evident for both scalar- and vector-averaged wind speed. The vertical velocity component shows a tendency to increase during an event (76%; Fig. 3c) and we will return to this below.

The frequency distribution of temperature changes (Fig. 3d) shows a tendency to decrease (74%), which includes a few especially large temperature changes. This is consistent with Mahrt (2010), where in stable conditions the strongest wind-direction shift tends to occur with a sharp decrease of temperature (a cold microfront).

4.2 Effects of Temperature

Relatively large oscillations of air temperature are quite common in the very stable regime (Mahrt 2014), and here we look at the effects of temperature increase and decrease on the vertical motion and turbulence during an event. The samples have been separated according to the sign of the temperature derivative during the central event and then composited according to the temperature decrease or increase. Table 3 shows the number of cases for each group. The temperature decrease is considerably more frequent for these large and sudden wind-direction shifts. Additionally, the cases with decreasing temperature tend to be associated with somewhat larger mean wind speeds.

Both the composite structure of the vertical velocity component and its variance reveal a clear difference between increasing and decreasing temperature cases (Fig. 5). The most conspicuous characteristic is that rising motion is found when the temperature decreases (Fig. 5a), followed by a positive change in the vertical velocity variance corresponding to an increase in turbulence intensity (Fig. 5b). As the composite structure is based on 1-min averages, this does not include small overturning events at, or immediately behind, the temperature decrease. These results for the decreasing temperature are in agreement with

Table 3 Number of cases and mean speeds ($m\,s^{-1}$) for wind and propagation, separated by the effects of temperature

	All cases		Propagation cases		
	n	Wind speed	*n*	Wind speed	Propagation speed
$dT/dt < 0$	96	1.0	51	1.1	3.8
$dT/dt > 0$	34	0.7	18	0.7	2.6

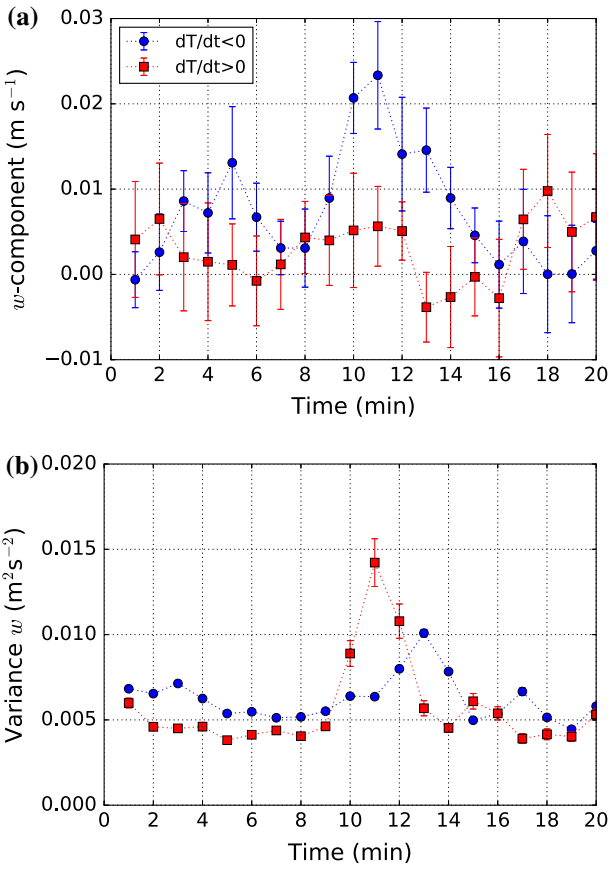

Fig. 5 Composited structure separated by increasing and decreasing temperature of, **a** vertical velocity component, and **b** variance of the vertical velocity component for the central events detected at the main station. Error bars show ± one standard error

Mahrt (2010), who observed that the maximum rising motion is above the cold microfront. In contrast, positive changes of temperature exhibit an increase of mixing during the sudden wind-direction shift and sinking motion closely following the shift. Again, these results are consistent with Mahrt (2010), who found that warm microfronts are associated with sinking motion in the warm air behind the microfront, suggesting that advection and downward mixing of air with higher momentum and higher temperatures could produce such warm microfronts. It is interesting to note that positive changes of temperature, which are associated

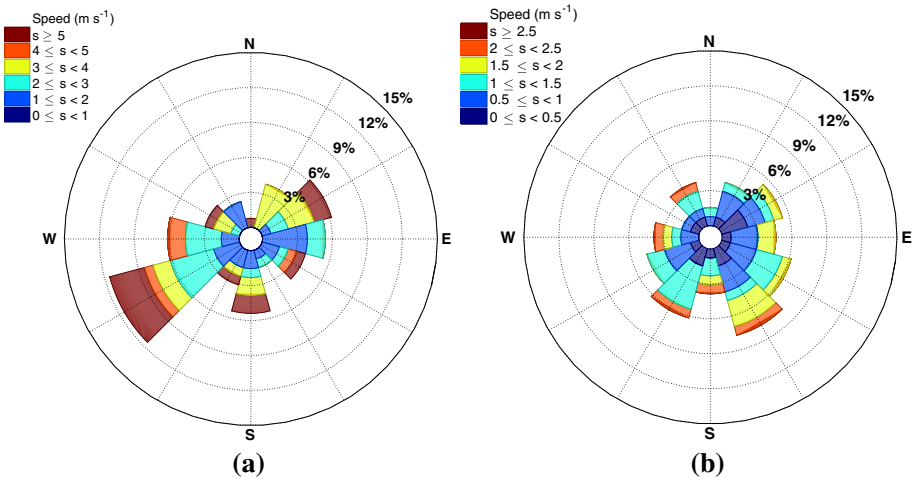

Fig. 6 Roses of **a** propagation of the central events and **b** the corresponding mean wind speed at the main station for the 3-month period

with increased mixing after the microfront passage, have a tendency to develop clockwise wind-direction shifts, with 65% of the cases exhibiting this behaviour. This result is not consistent with the hypothesized effects of downward mixing assuming Ekman turning in the ABL. However, a more detailed analysis would require vertical profiles of the wind direction, which were not available for this field experiment. The opposite behaviour is found for negative temperature changes, with 63% of the cases having counter-clockwise shifts.

5 Propagation of Structures

5.1 Direction and Speed of Propagation

Of the original 130 samples, 84 remained after the minimum cross-correlation constraint was applied. The constraint was applied to any combination of three station towers, even though all four stations were available for this period. To make the selection of cases more robust, all four combinations of three station towers were tested. We required that at least two of the four combinations to be within 30° and $2\,\mathrm{m\,s^{-1}}$ of each other. We then used the average of these "consistent" combinations to obtain a single value for the speed and direction for a sample. This additional "consistency" constraint further reduced the number of useful samples to 69.

A "propagation rose" for these 69 samples (Fig. 6a) displays a strong south-westerly preference despite the mostly homogeneous, flat terrain. Overall, the average propagation speed for the 69 samples is $3.5\,\mathrm{m\,s^{-1}}$ with approximately 72% of these events having propagation speeds between 1 and $4\,\mathrm{m\,s^{-1}}$. Few samples reach speeds greater than $10\,\mathrm{m\,s^{-1}}$.

It is important to examine whether the propagation is related to the mean wind vector. The wind rose for the 69 samples (Fig. 6b) does not display any strong preference for wind direction and is not similar to the propagation rose. Rees and Mobbs (1988) found similar results for gravity waves at Halley Base, Antarctica. The distribution of the difference between propagation speed and wind speed (Fig. 7) displays a clear tendency for the propagation speed

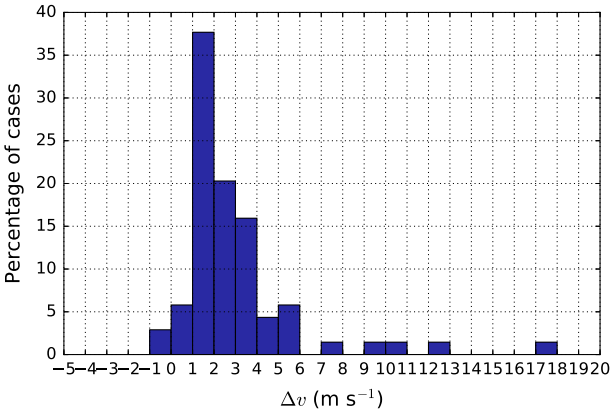

Fig. 7 Frequency distribution of differences between the propagation speed and the corresponding mean wind speed (Δv) at the main station for the 3-month period

to be greater than the wind speed. The correlation coefficient between the propagation and wind speed is -0.005, and the correlation coefficient between the propagation and wind direction is -0.12, which does not support any relationship between the propagation and the mean wind speed.

The effects of temperature on the propagation speed are shown in Table 3, and as in the previous analysis with all the samples, decreasing temperature exhibits a larger number of cases and somewhat larger mean wind speeds. Propagation speed follows this behaviour and the events propagate more rapidly when temperature decreases.

5.2 Complete Period of Measurements

Here we perform the same analysis as above, except for the entire period when the three satellite stations were operating (22 months). The main station is substituted by station 1 to detect wind-direction-shift events, with a total of 1565 wind-direction-shift events and 861 sampling windows found at station 1. Using the same threshold of 0.7 for the cross-correlation coefficient as before, 736 samples are obtained for the calculation of speed and direction of propagation. No additional "consistency" criteria can be applied.

Figure 8 shows both the propagation and mean wind roses for the 736 samples. As before, there is no clear relationship between either the propagation and mean wind direction or the propagation and mean wind speed. The absolute values of correlation coefficient for speed and direction between propagation and mean wind vectors are less than 0.15. The propagation speeds are again most of the time greater than wind speed, with values of wind speed $<5\,\mathrm{m\,s^{-1}}$ and some values of propagation speed reaching $30\,\mathrm{m\,s^{-1}}$. While there is still a clear preference for a south-westerly direction for the propagation direction, there is now a much stronger preference for a north-easterly origin. One could speculate that the predominance of north-easterly propagation directions is related to a 20-m hill located 15 km north-east of the network. Sun et al. (2015a) found that for the relatively flat CASES-99 site, the changes in wind speed and temperature were generated by internal gravity waves resulting from cold currents associated with small terrain irregularities.

The complete period of measurements allowed the analysis of the seasonal variability of wind-direction shifts. The seasonal cycle of the number of wind-direction shifts per night (Fig. 9a) peaks during the cold season (JJA) and has a minimum during the warm season

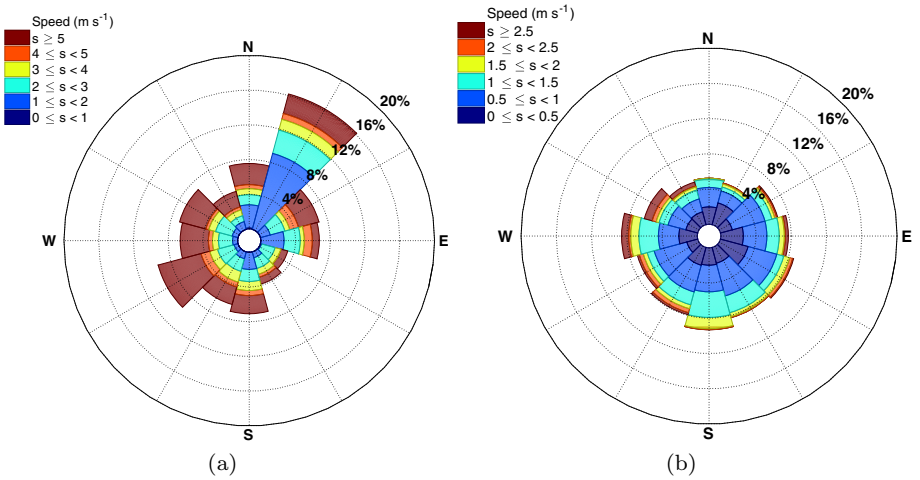

Fig. 8 Roses for the complete observational period of **a** propagation of the central events and **b** the corresponding mean wind speed at station 1

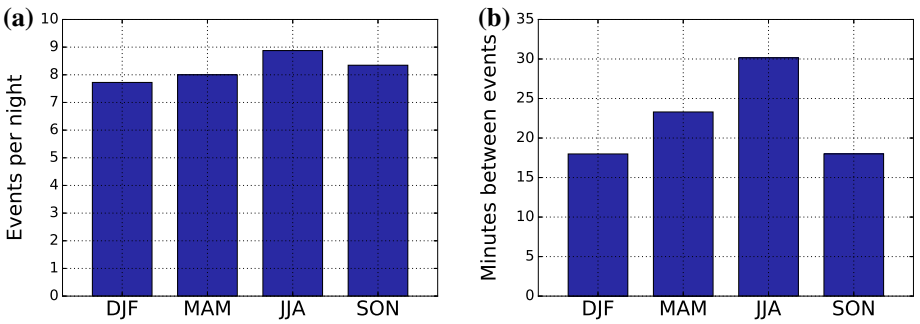

Fig. 9 Seasonal variability of **a** the average number of wind-direction shifts per night and **b** the average time (minutes) between wind-direction shifts

(DJF). The variability of the number of events is larger between years than seasons (not shown). A stronger seasonal variability is present for the time between events, where the mean time between events increases from 18 min in the warm season to 30 min in the cold season (Fig. 9b).

The propagation direction of the samples exhibits a noticeable seasonal cycle (Fig. 10). During seasons JJA and SON there is a strong tendency of wind-direction shifts to develop and propagate from the north-east, similar to the overall mean. During DJF the propagation is predominantly from the south-west, which is similar to the propagation during the 3-month period (Fig. 7) of all four towers operating; The MAM season is as a transitional period between the warm and cold seasons. Figure 11 shows the corresponding mean wind roses for each season. Although the mean wind exhibits some seasonal changes, there is still no obvious relationship between it and the propagation vector.

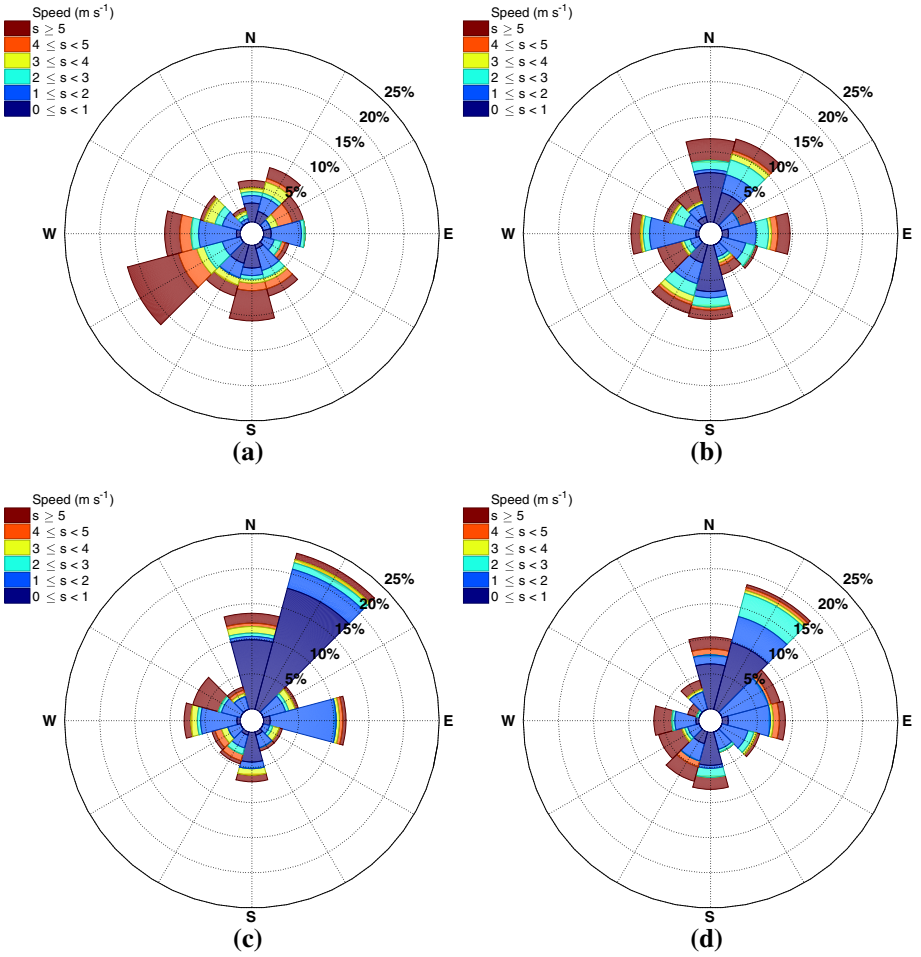

Fig. 10 Seasonal roses of propagation of the central events at station 1 for the complete observational period: **a** DJF, **b** MAM, **c** JJA, and **d** SON

6 Discussion and Conclusions

A horizontal network of high-resolution measurements in north-western Victoria, Australia is used to estimate statistics of submeso motions over an area with relatively homogeneous and flat terrain. The submeso motions at this site exhibit behaviour typical for this type of terrain, such as the lower relative mesovelocity scale and smaller cross-wind variances than for complex terrain. These results corroborate the hypothesis that local surface features, such as terrain complexity and surface heterogeneity, influence submeso processes.

The wind-direction variability in stable conditions was analyzed by extracting individual events with large and sudden wind-direction shifts. The large sudden wind-direction shifts have a tendency to develop with a decrease in air temperature (74% of time). These events are associated with rising motions when the temperature decreases, suggesting that an external

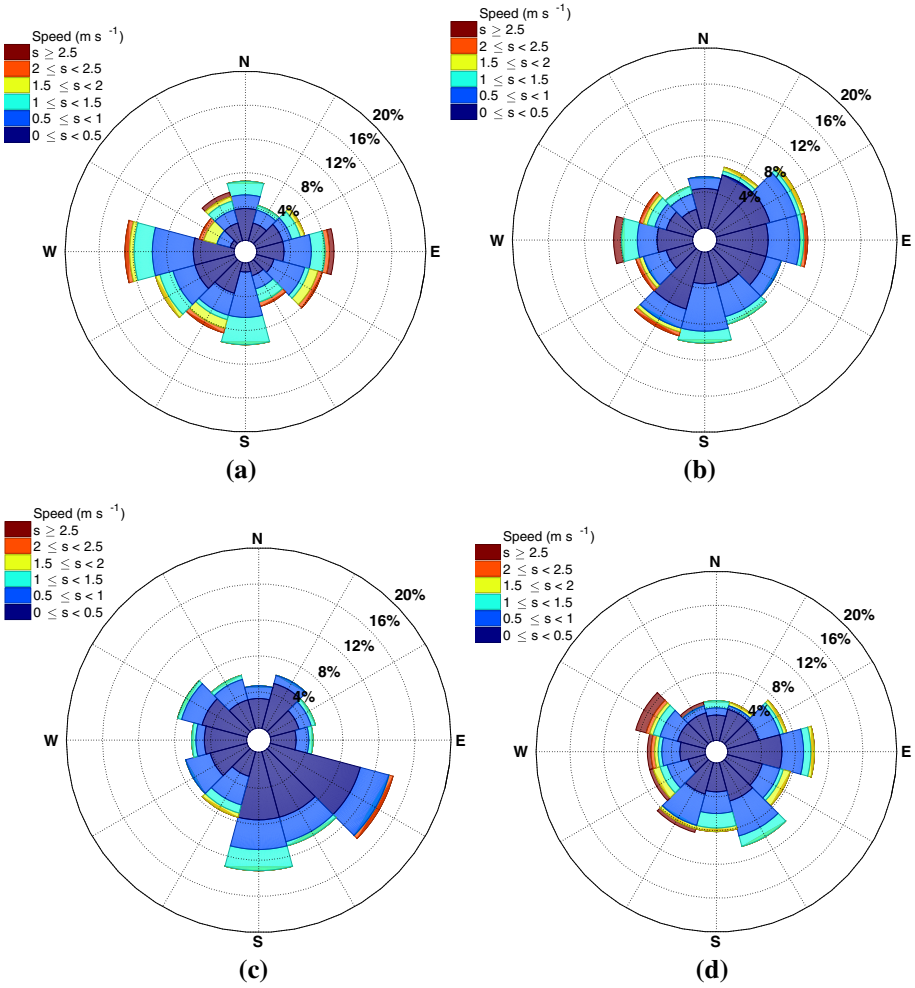

Fig. 11 As Fig. 11, except showing the roses of mean wind speed corresponding to the central events

source of energy is required to maintain these thermal circulations. Characteristics of large changes in wind direction are consistent with previous studies (e.g., Mahrt 2007, 2008).

The horizontal propagation of the wind-direction shifts was analyzed using the cross-correlation function method. The propagation directions show a preference for directions from the south-west during the 3-month period. However, when the entire dataset of 22 months is considered, the preference shifts to a north-easterly direction, although with considerable seasonal variability. A potential source of events propagating from the north-east could be related to the 20-m hill located about 15 km to the north-east of the network, while the south-westerly propagation might be related to the 30-m hill located about 30 km to the south-west. If true, this would imply that disturbances generated by small obstacles in a stable boundary layer propagate several tens of km and produce large and sudden wind-direction shifts, together with the associated effects analyzed herein. Such behaviour would preclude strictly

local parametrization of submeso motions in numerical models. Further analysis is needed to confirm the generality of such mechanisms.

Propagation speeds tend to be greater than the mean wind speed for all the cases analyzed. There is no relationship between the propagation vector and the mean wind vector, indicating that the events are not flow perturbations advected by the local flow. Hence the Taylor hypothesis is not applicable, and no inference can be made about the spatial structure of submeso motions from time series. This indicates that developing a suitable parametrization in numerical models might require different techniques and observations than are typically available from point measurements. Furthermore, if the observed relationship between the terrain complexity and submeso variability can be quantified, parametrizations could be developed that are based on the characteristics of the model subgrid-scale terrain.

Acknowledgements We are grateful to four anonymous reviewers for useful and constructive comments that helped to improve the manuscript.

References

Acevedo OC, Costa FD, Oliveira PES, Puhales FS, Ga Degrazia, Roberti DR (2014) The influence of submeso processes on stable boundary layer similarity relationships. J Atmos Sci 71(1):207–225

Anfossi D, Oettl D, Degrazia G, Goulart lA (2005) An analysis of sonic anemometer observations in low wind speed conditions. Boundary-Layer Meteorol 114(1):179–203

Belušić D, Güttler I (2010) Can mesoscale models reproduce meandering motions? Q J R Meteorol Soc 136(648):553–565

Belušić D, Mahrt L (2008) Estimation of length scales from mesoscale networks. Tellus A 60(4):706–715

Belušić D, Mahrt L (2012) Is geometry more universal than physics in atmospheric boundary layer flow? J Geophys Res Atmos 117:d09115. doi:10.1029/2011JD016987

Cava D, Mortarini L, Giostra U, Richiardone R, Anfossi D (2016) A wavelet analysis of low-wind-speed submeso motions in a nocturnal boundary layer. Q J R Meteorol Soc. doi:10.1002/qj.2954

Grachev AA, Fairall CW, Persson POG, Andreas EL, Guest PS (2005) Stable boundary-layer scaling regimes: the SHEBA data. Boundary-Layer Meteorol 116(2):201–235

Güttler I, Belušić D (2012) The nature of small-scale non-turbulent variability in a mesoscale model. Atmos Sci Lett 13(3):169–173

Hande L, Siems S, Manton M, Belusic D (2012) Observations of wind shear over the southern ocean. J Geophys Res Atmos 117:d12206. doi:10.1029/2012JD017488

Kang Y, Belušić D, Smith-Miles K (2015) Classes of structures in the stable atmospheric boundary layer. Q J R Meteorol Soc 141:2057–2069. doi:10.1002/qj.2501

Mahrt L (2007) Weak-wind mesoscale meandering in the nocturnal boundary layer. Environ Fluid Mech 7(4):331–347

Mahrt L (2008) Mesoscale wind direction shifts in the stable boundary-layer. Tellus A 60(4):700–705

Mahrt L (2010) Common microfronts and other solitary events in the nocturnal boundary layer. Q J R Meteorol Soc 136(652):1712–1722

Mahrt L (2014) Stably stratified atmospheric boundary layers. Annu Rev Fluid Mech 46:23–45

Monserrat S, Thorpe AJ (1992) Gravity-wave observations using an array of microbarographs in the Alearic Islands. Q J R Meteorol Soc 118(504):259–282

Monti P, Fernando HJS, Princevac M, Chan WC, Kowalewski TA, Pardyjak ER (2002) Observations of flow and turbulence in the nocturnal boundary layer over a slope. J Atmos Sci 59(17):2513–2534

Mortarini L, Stefanello M, Degrazia G, Roberti D, Castelli ST, Anfossi D (2016) Characterization of wind meandering in low-wind-speed conditions. Boundary-Layer Meteorol. doi:10.1007/s10546-016-0165-6

Poulos GS, Blumen W, Fritts DC, Lundquist JK, Sun J, Burns SP, Nappo C, Banta R, Newsom R, Cuxart J et al (2002) CASES-99: a comprehensive investigation of the stable nocturnal boundary layer. Bull Am Meteorol Soc 83(4):555–581

Rees JM, Mobbs SD (1988) Studies of internal gravity waves at Halley Base, Antarctica, using wind observations. Q J R Meteorol Soc 114(482):939–966

Sandu I, Beljaars A, Bechtold P, Mauritsen T, Balsamo G (2013) Why is it so difficult to represent stably stratified conditions in numerical weather prediction (NWP) models? J Adv Model Earth Syst 5(2):117–133

Suarez A, Stauffer DR, Gaudet BJ (2015) Wavelet-based methodology for the verification of stochastic submeso and meso-gamma fluctuations. Mon Weather Rev 143(10):4220–4235

Sun J, Lenschow DH, Mahrt L, Nappo C (2013) The relationships among wind, horizontal pressure gradient, and turbulent momentum transport during CASES-99. J Atmos Sci 70(11):3397–3414

Sun J, Mahrt L, Nappo C, Lenschow DH (2015a) Wind and temperature oscillations generated by wave-turbulence interactions in the stably stratified boundary layer. J Atmos Sci 72(4):1484–1503

Sun J, Nappo CJ, Mahrt L, Belušić D, Grisogono B, Stauffer DR, Pulido M, Staquet C, Jiang Q, Pouquet A et al (2015b) Review of wave-turbulence interactions in the stable atmospheric boundary layer. Rev Geophys 53(3):956–993

Vercauteren N, Klein R (2015) A clustering method to characterize intermittent bursts of turbulence and interaction with submesomotions in the stable boundary layer. J Atmos Sci 72(4):1504–1517

Vercauteren N, Mahrt L, Klein R (2016) Investigation of interactions between scales of motion in the stable boundary layer. Q J R Meteorol Soc. doi:10.1002/qj.2835

Vickers D, Mahrt L (2007) Observations of the cross-wind velocity variance in the stable boundary layer. Environ Fluid Mech 7(1):55–71

Vickers D, Mahrt L, Belušić D (2008) Particle simulations of dispersion using observed meandering and turbulence. Acta Geophys 56(1):234–256

Wilczak JM, Oncley SP, Stage SA (2001) Sonic anemometer tilt correction algorithms. Boundary-Layer Meteorol 99(1):127–150